Aerospace Information Research Institute(AIR)
Chinese Academy of Sciences(CAS)

Aerosol polarization radiative transfer simulation and retrieval for DPC/GF-5

Zhengqiang Li*, Yisong Xie, Weizhen Hou

*E-mail: lizq@radi.ac.cn

May 1, 2019

Outline

- **1. Polarimetric satellite remote sensing**
- 2. Inversion framework for DPC/GF-5
- 3. Aerosol retrieval & preliminary validation

Climate & Environment Satellite Programs in China

- ✓ **High resolution (GF) program : 7 civil satellites**
- ✓ **Space Infrastructure (SI) program: 50+ satellites**

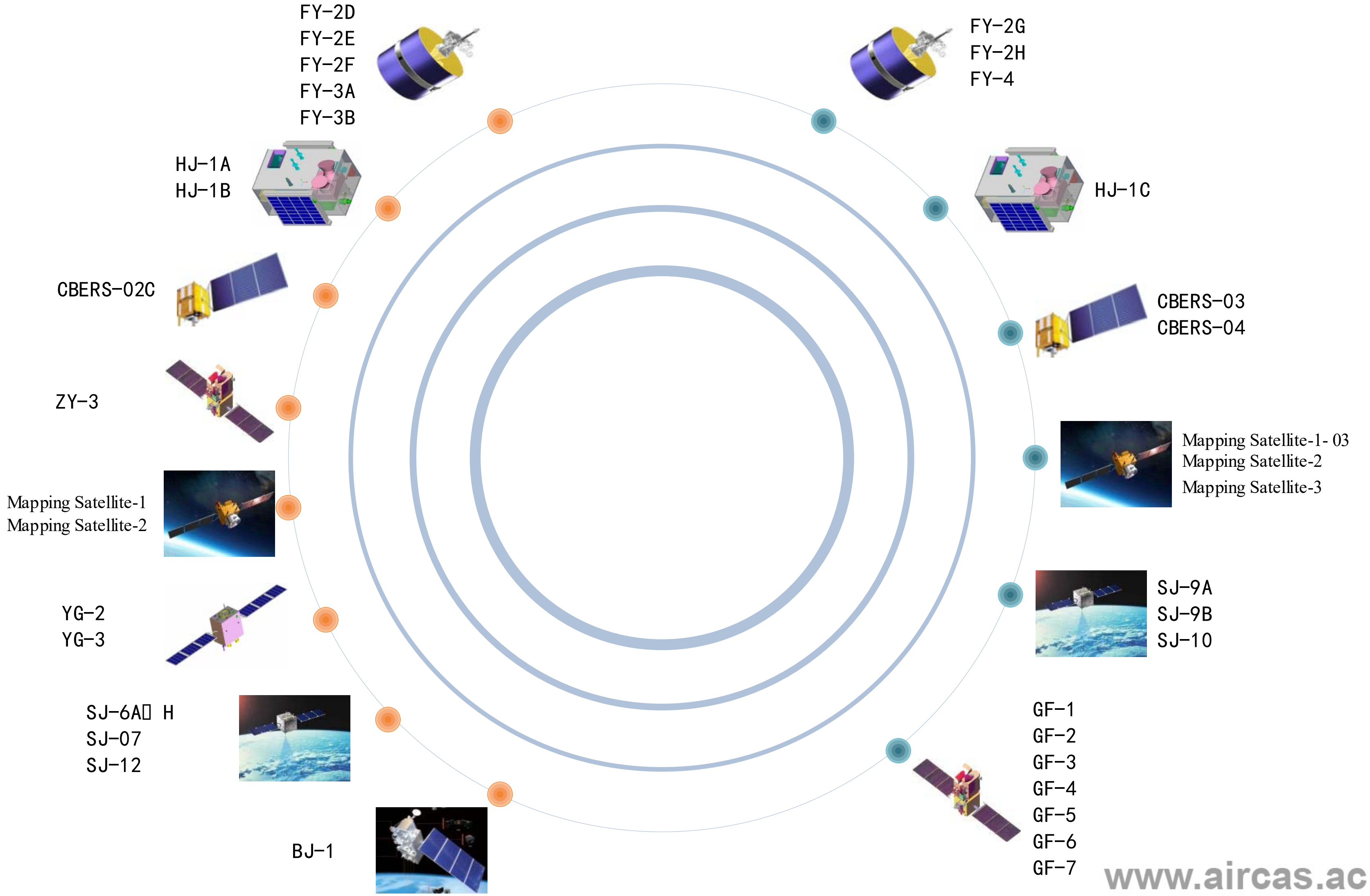

➢ Satellite instruments for polarimetric remote sensing

APS/Glory, NASA/USA

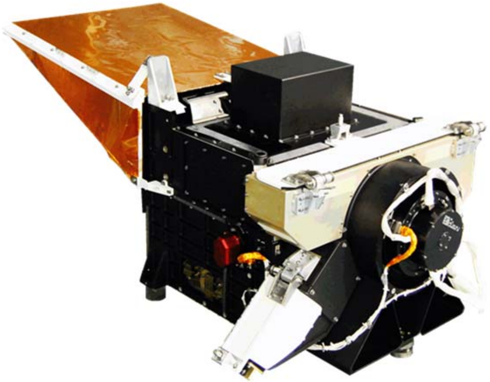

3MI, EUMETSAT/EU

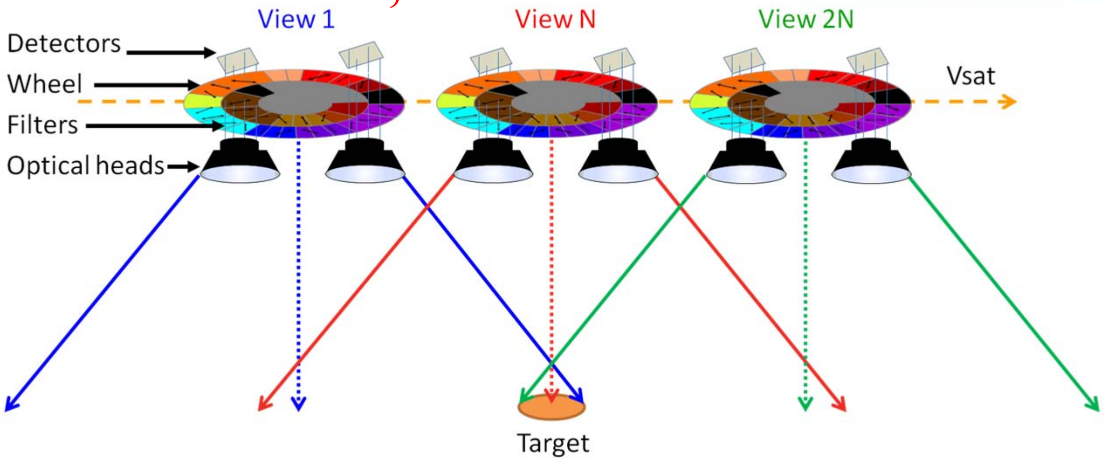

MAIA/OTB-2, NASA/USA

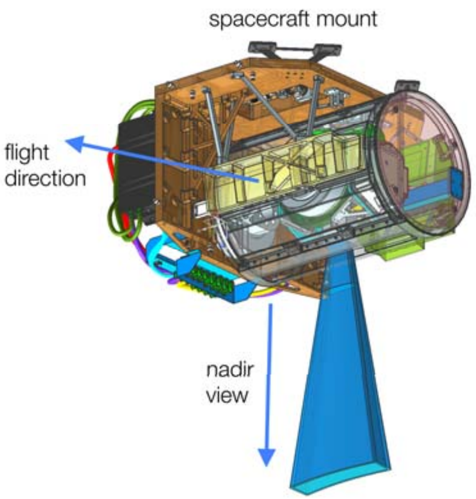

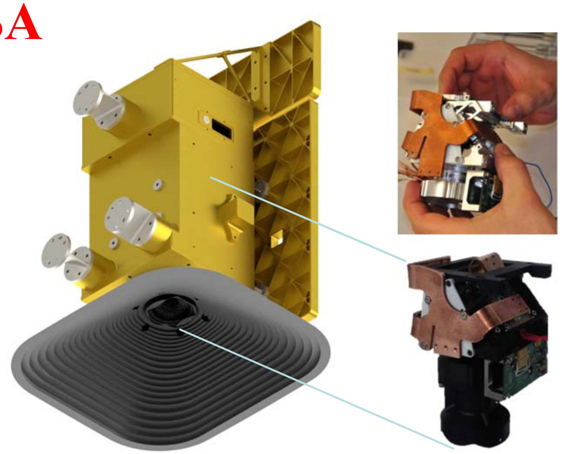

HARP2/PACE, UMBC/USA

DPC/GF-5, China

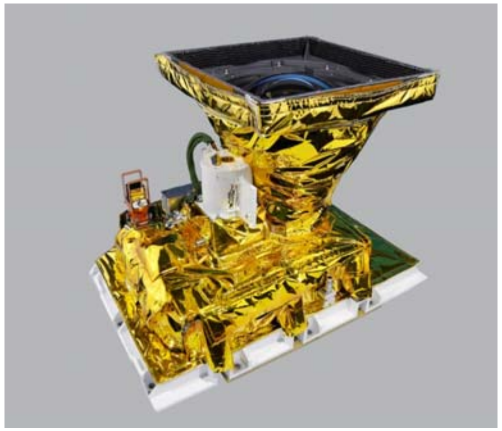

Dubovik, O. & Li, Z., et al. (2019), Polarimetric remote sensing of atmospheric aerosols: Instruments, methodologies, results, and perspectives, *JQSRT*, *224*, 474-511

➢ Airborne instruments for polarimetric RS

RSP, NASA/USA

AirMSPI-2, NASA/USA

Airborne DPC, China

SMAC, China

AirHARP, UMBC/USA

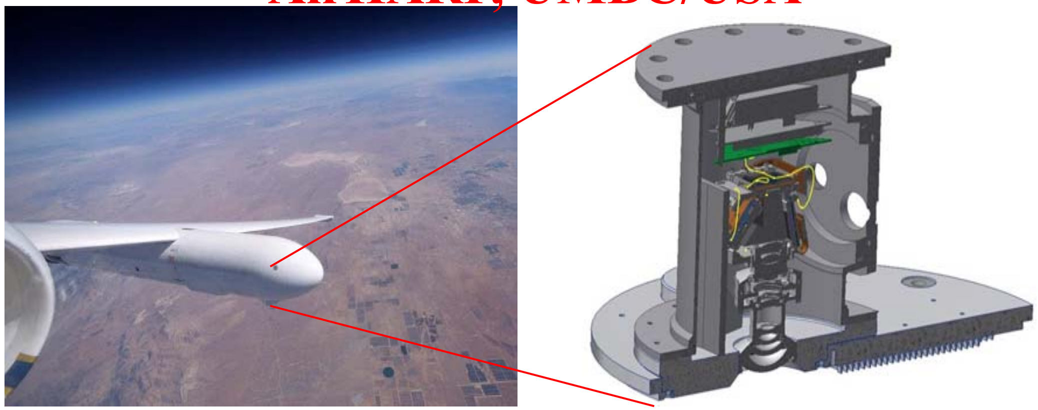

AMPR, China

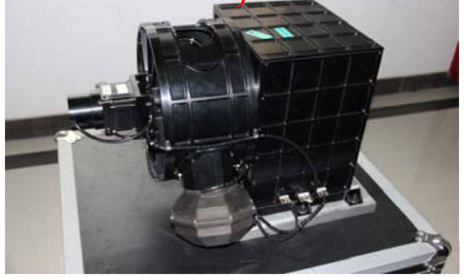

Dubovik, O. & Li, Z., et al. (2019), Polarimetric remote sensing of atmospheric aerosols: Instruments, methodologies, results, and perspectives, *JQSRT*, *224*, 474-511

➤ GF-5 satellite

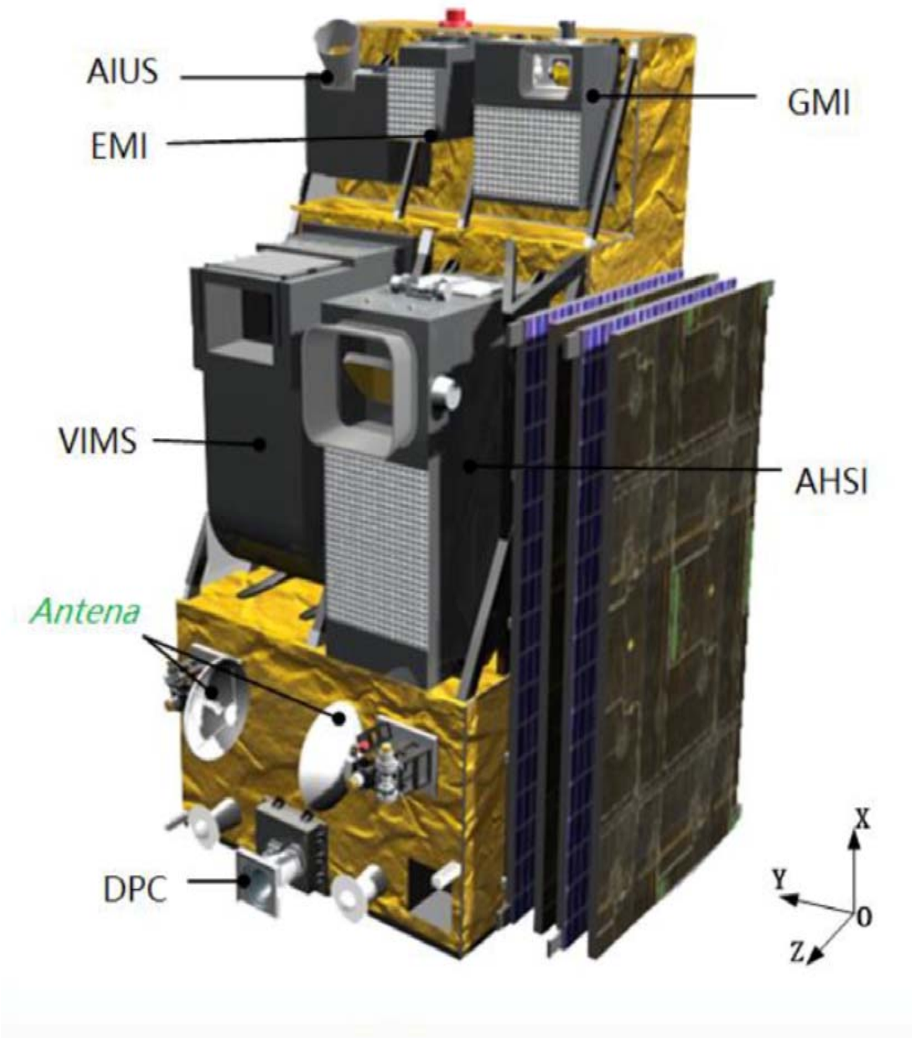

Sensor	Full Name
AHSI	Advanced Hyperspectral Imager
VIMS	Visual and Infrared Multispectral Sensor
AIUS	Atmospheric Infrared Ultra-spectral Sensor
EMI	Environment Monitoring Instrument
GMI	Greenhouse-gases Monitoring Instrument
DPC	Directional Polarization Camera

Li, Z., et al. (2018), **Directional Polarimetric Camera (DPC): Monitoring aerosol spectral optical properties over land from satellite observation,** ***JQSRT*****, *218*, 21-37**

➢ GF-5 satellite

May 9, 2018, 02:28, Taiyuan

➢ Directional Polarimetric Camera (DPC)

Optical head of DPC/GF-5

Band & polarization configuration

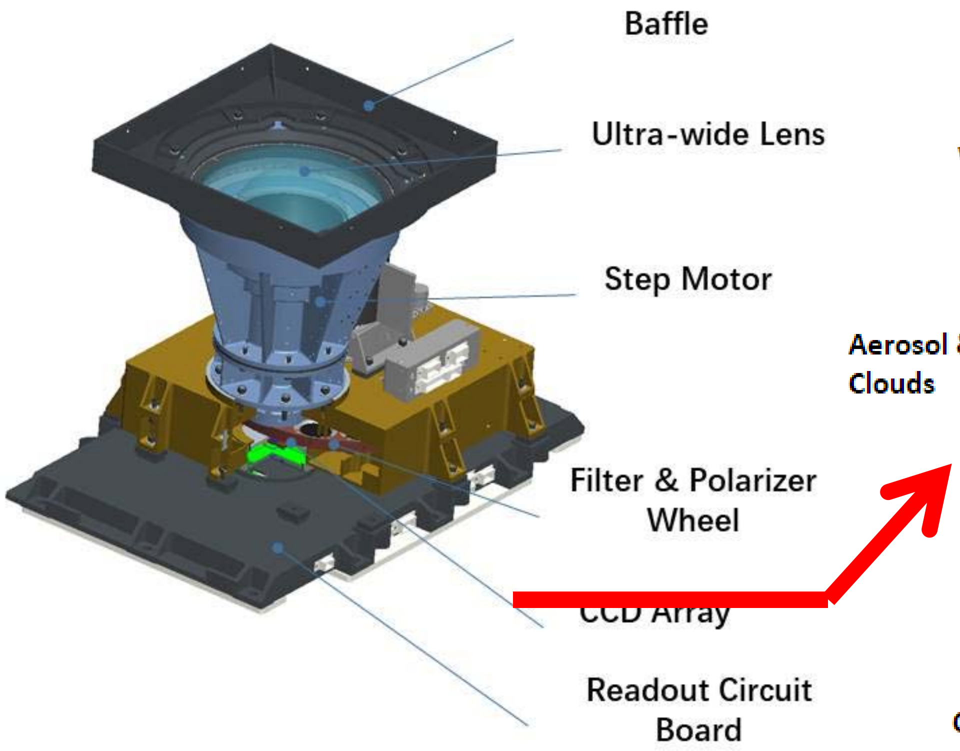

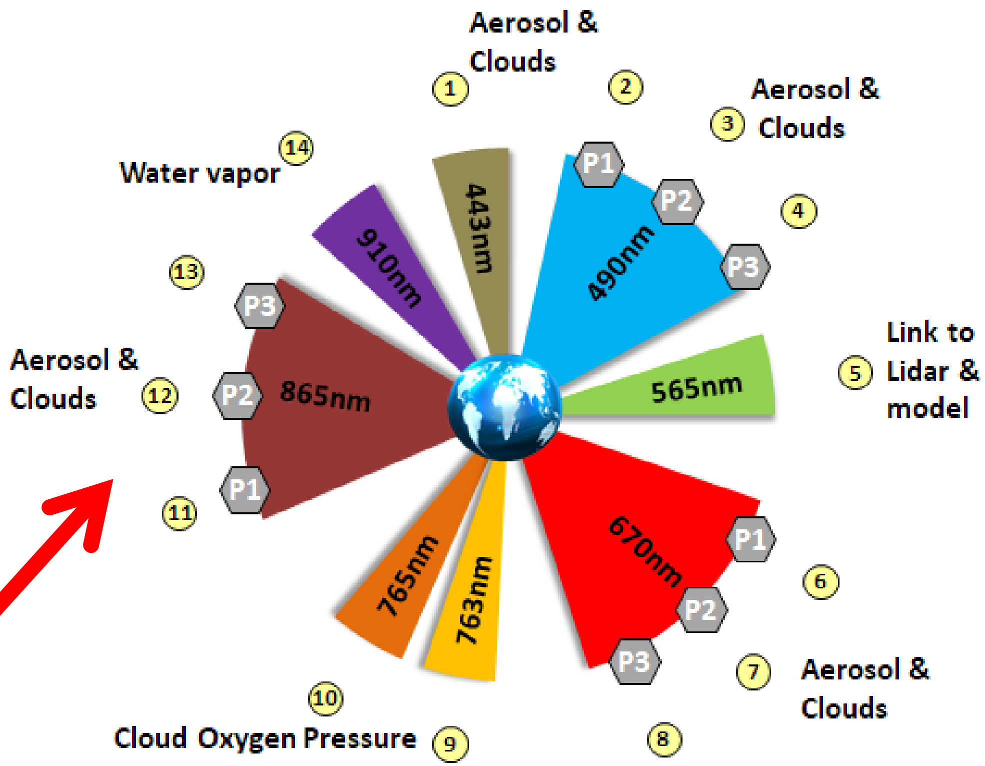

Li, Z., et al. (2018), Directional Polarimetric Camera (DPC): Monitoring aerosol spectral optical properties over land from satellite observation, *JQSRT*, *218*, 21-37

➢ Directional Polarimetric Camera (DPC)

Parameter	Value	Parameter	Value
Instrument FOV	±50°	Polarized angle	0°, 60°, 120°
Spatial res. (km)	3.3	Stokes	I, Q, U
Swath width (km)	1850	Rad. Cal. Error	≤ 5%
Multi-angle	≥ 9	Pol. Cal. Error	≤ 0.02
Image pixels	512×512	Band width	20, 20, 20, 20, 10, 40, 40, 20 nm
Spectral band	443, 490(P), 565, 670(P), 763,765, 865(P), 910 nm (**P for polarization**)		

✓ The DPC is the first Chinese multi-angle polarized earth observation satellite sensor, which is the type of POLDER polarimetric imager

➢ Intensity and polarization measurements

MODIS_2018-06-12-05:30
(Intensity)

DPC_2018-06-12-04:40
(Intensity)

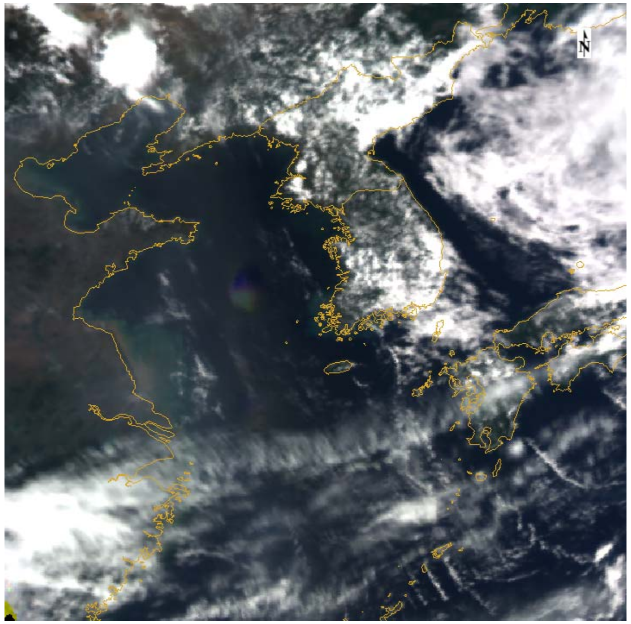

DPC_2018-06-12-04:40
(Polarization)

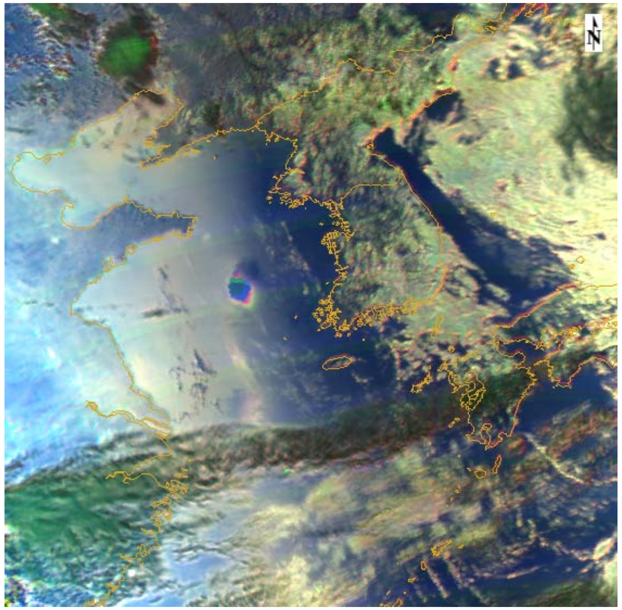

MODIS

DPC/GF-5

Outline

- 1. Polarimetric satellite remote sensing
- **2. Inversion framework for DPC/GF-5**
- 3. Aerosol retrieval & preliminary validation

➢ Multi-angle measurements of DPC

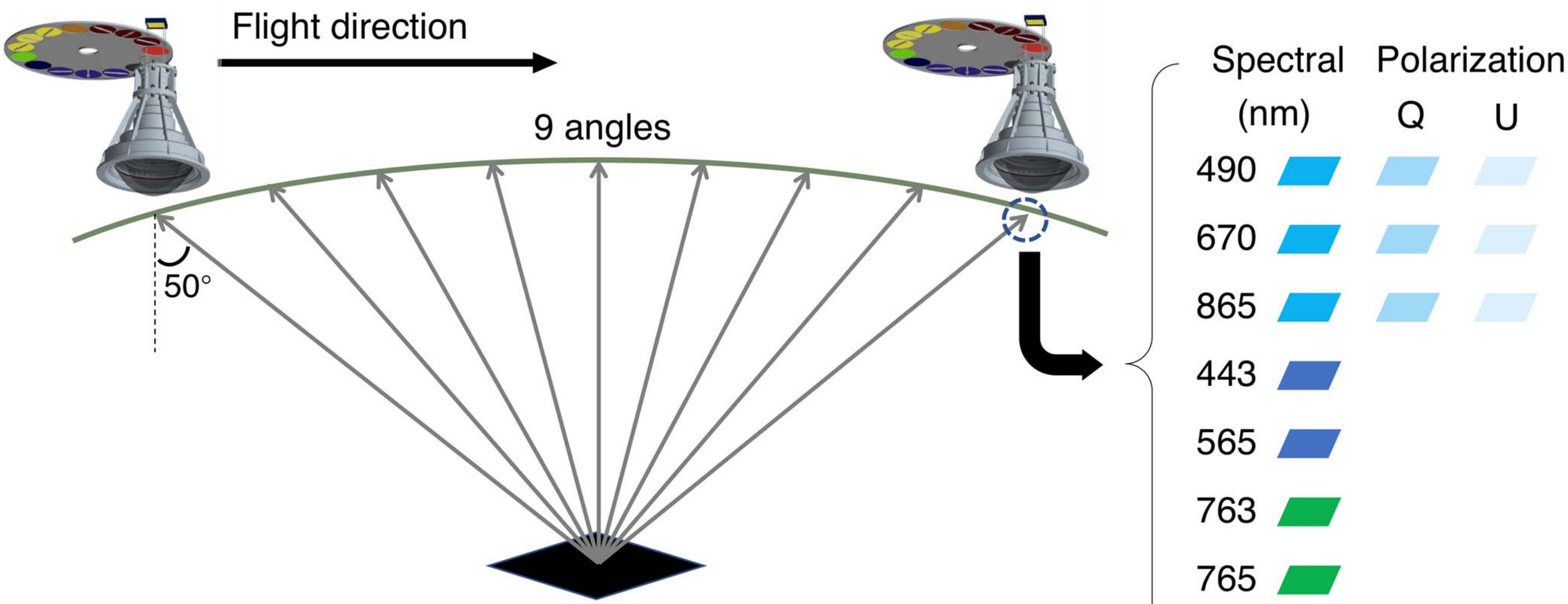

Total measurements in 1 pixel:
9 angles × (8 spectral + 3 polarization × 2) = 126

✓ By taking the measurements with 9 viewing angles as an example, the multi-angle observation principle and the description of measurement dataset of DPC are described.

➢ Ill-conditioning in inversion

y: Observation vector

x: State vector (unknowns, aerosol & surface parameters to be retrieved)

$\mathbf{x} \in \left[V_0^{\mathrm{f}}, V_0^{\mathrm{c}}, f(\lambda), k_1, k_2, C, r_{\mathrm{eff}}^{\mathrm{f}}, v_{\mathrm{eff}}^{\mathrm{f}}, r_{\mathrm{eff}}^{\mathrm{c}}, v_{\mathrm{eff}}^{\mathrm{c}}, m_{\mathrm{r}}^{\mathrm{f}}(\lambda), m_{\mathrm{i}}^{\mathrm{f}}(\lambda), m_{\mathrm{r}}^{\mathrm{c}}(\lambda), m_{\mathrm{i}}^{\mathrm{c}}(\lambda)\right]^T$

Case of DPC/GF-5: No. of bands (λ) is 5 ⟶ No. of *x* elements is 34!

$$\mathbf{y} = \mathbf{F}(\mathbf{x}) + \epsilon$$

So many unknowns to be retrieved!

If number of y elements < that of x: ill-conditioning problem

Radiative transfer simulation

UNL-VRTM

www.unl-vrtm.org

UNL-VRTM Features

Unified Linearized Vector Radiative Transfer Model

$$\mathbf{S} = \begin{bmatrix} I \\ Q \\ U \\ V \end{bmatrix}$$

Vector RTM for simulation of light intensity and polarization

Accurate UV-to-IR (0.2 - 40 micron) hyperspectral RTM

$$\mathbf{J} = \begin{bmatrix} \frac{\partial F_1}{\partial x_1} & \cdots & \frac{\partial F_1}{\partial x_n} \\ \vdots & \ddots & \vdots \\ \frac{\partial F_m}{\partial x_1} & \cdots & \frac{\partial F_m}{\partial x_n} \end{bmatrix}.$$

Online analytical Jacobian of Stokes to particle, gas, and surface properties

Information content analysis for future satellite sensors

Flexible and easy-to-read modular Fortran programing

python™ Package Index

Complementary Python utility package, pyunlvrtm

(Wang et al., JQSRT, 2015; Xu & Wang, JGR, 2015)

➢Inversion framework

❖ **Forward model** (Rodgers, 2000):

$$\mathbf{y} = \overbrace{\mathbf{F}}^{\text{UNL-VRTM}}(\mathbf{x}) + \boldsymbol{\varepsilon}$$

❖ **State vector** (retrieval parameters):

$$\mathbf{x} = \Big[\overbrace{V_0^{\mathrm{f}}, V_0^{\mathrm{c}}}^{\text{Aerosol volume concentration}}, \overbrace{f(\lambda_1), \cdots, f(\lambda_5), k_1, k_2}^{\text{Improve BRDF parameter}}, \overbrace{C}^{\text{BPDF parameter}}\Big]^T$$

❖ **Aerosol model** (a priori):

$$\mathbf{b} = \Big[\underbrace{r_{\mathrm{eff}}^{\mathrm{f}}, v_{\mathrm{eff}}^{\mathrm{f}}, r_{\mathrm{eff}}^{\mathrm{c}}, v_{\mathrm{eff}}^{\mathrm{c}}}_{\text{Size distribution for fine \& coarse}}, \underbrace{m_{\mathrm{r}}^{\mathrm{f}}(\lambda), m_{\mathrm{i}}^{\mathrm{f}}(\lambda), m_{\mathrm{r}}^{\mathrm{c}}(\lambda), m_{\mathrm{i}}^{\mathrm{c}}(\lambda)}_{\text{Refractive indices parameters for fine \& coarse}}\Big]^T$$

❖ **Cost function** (optimized):

$$J(\mathbf{x}) = \frac{1}{2}[\mathbf{y} - \mathbf{F}(\mathbf{x})]^T \mathbf{S}_\epsilon^{-1} [\mathbf{y} - \mathbf{F}(\mathbf{x})] + \frac{1}{2}(\mathbf{x} - \mathbf{x}_{\mathrm{a}})^T \mathbf{S}_{\mathrm{a}}^{-1} (\mathbf{x} - \mathbf{x}_{\mathrm{a}})$$

❖ **Gradient vector** (iteration):

$$\nabla_{\mathbf{x}} J(\mathbf{x}) = -\mathbf{K}^T \mathbf{S}_\epsilon^{-1} [\mathbf{y} - \mathbf{F}(\mathbf{x})] + \mathbf{S}_{\mathrm{a}}^{-1} (\mathbf{x} - \mathbf{x}_{\mathrm{a}}), \overbrace{\mathbf{K}_{j,i}}^{\text{Jacobians by UNL-VRTM}} = \frac{\partial y_j}{\partial x_i}, (i = 1, \cdots n; j = 1, \cdots, m)$$

➢ Inversion framework

❖ **Surface reflectance matrix** (Dubovik et al., 2011):

$$\boldsymbol{R}(\theta_0, \theta_\mathrm{v}, \varphi, \lambda) = \rho^s \begin{bmatrix} 1 & 0 & 0 & 0 \\ 0 & 0 & 0 & 0 \\ 0 & 0 & 0 & 0 \\ 0 & 0 & 0 & 0 \end{bmatrix} + \frac{\rho_\mathrm{Maignan}}{2} \begin{bmatrix} r_\mathrm{l}^2 + r_\mathrm{r}^2 & r_\mathrm{l}^2 - r_\mathrm{r}^2 & 0 & 0 \\ r_\mathrm{l}^2 - r_\mathrm{r}^2 & r_\mathrm{l}^2 + r_\mathrm{r}^2 & 0 & 0 \\ 0 & 0 & 2r_\mathrm{l}r_\mathrm{r} & 0 \\ 0 & 0 & 0 & 2r_\mathrm{l}r_\mathrm{r} \end{bmatrix}$$

❖ **Improved BRDF model** (Litvinov et al., 2011):

$$r_\lambda(\mu_0, \mu_v, \phi) = f(\lambda)[1 + k_1 f_\mathrm{geom}(\mu_0, \mu_v, \phi) + k_2 f_\mathrm{vol}(\mu_0, \mu_v, \phi)]$$

❖ **BPDF model** (Maignan et al., 2009):

$$R_p^s(\theta_0, \theta_\mathrm{v}, \varphi) = \rho_\mathrm{Maignan}\, F_p(\gamma, n_i) = \frac{C \exp[\tan(\gamma)] \exp(NDVI)}{\cos(\theta_0) + \cos(\theta_\mathrm{v})} F_p(\gamma, n_i)$$

➢ Inversion framework

❖ **Spectral aerosol optical depth (AOD):**

$$\tau_a(\lambda) = \tau_a^f(\lambda) + \tau_a^c(\lambda) = \frac{3V_0^f}{4r_{eff}^f} Q_{ext}^f(\lambda) + \frac{3V_0^c}{4r_{eff}^c} Q_{ext}^c(\lambda)$$

❖ **Angstrom exponent (α)**

$$\alpha = \ln\frac{\tau_a(\lambda_p)}{\tau_a(\lambda_q)} \Big/ \ln\frac{\lambda_q}{\lambda_p}$$

❖ **Fine-mode fraction (FMF):**

$$\mathrm{FMF}(\lambda) = \tau_a^f(\lambda) / \tau_a(\lambda)$$

➢ Multi-viewing observation geometries for forward simulations

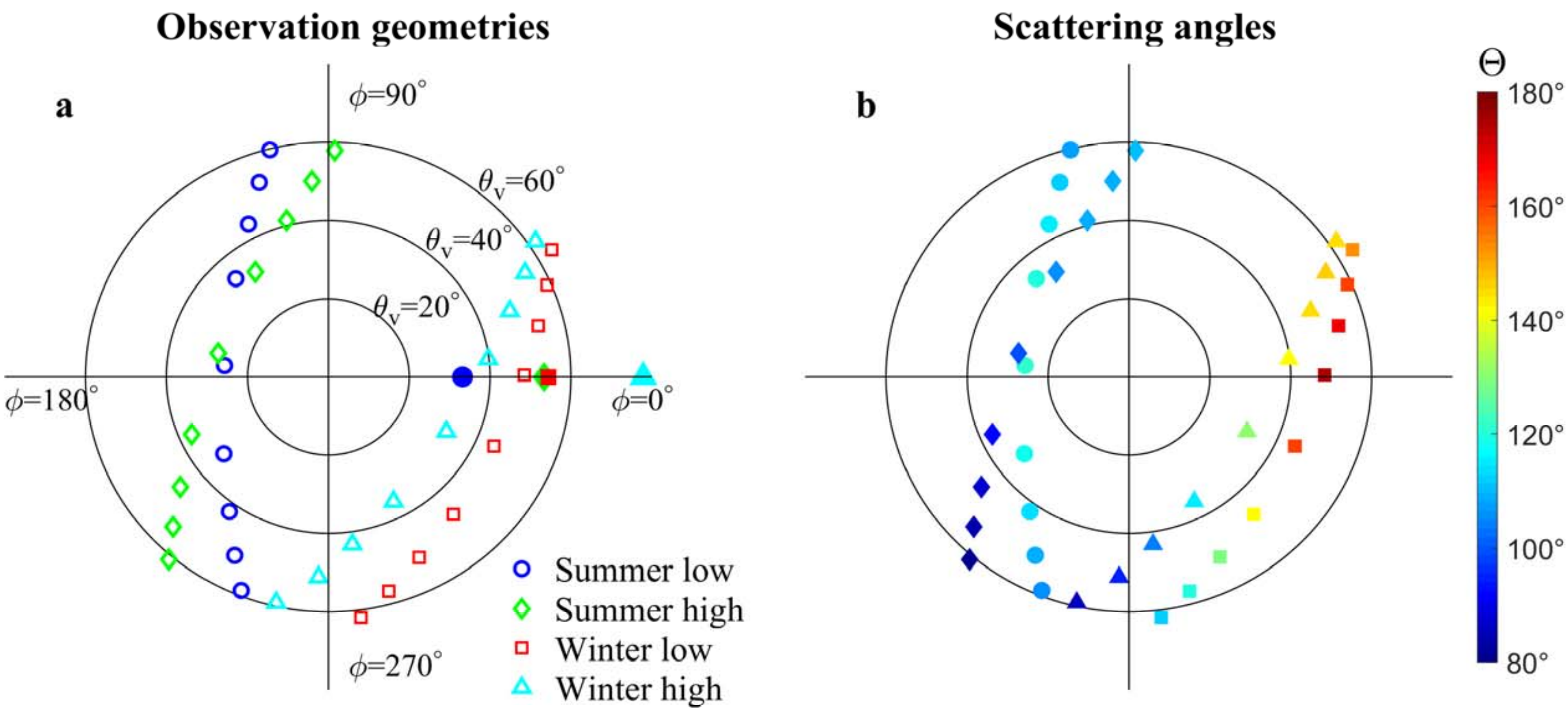

✓ 4 multi-viewing observation geometries are considered with the combinations of different solar zenith angles (θ_0), viewing zenith angles (θ_v) and relative azimuth angles (ϕ) to represent the typical observations in different location.

➢ Aerosol model used for simulations

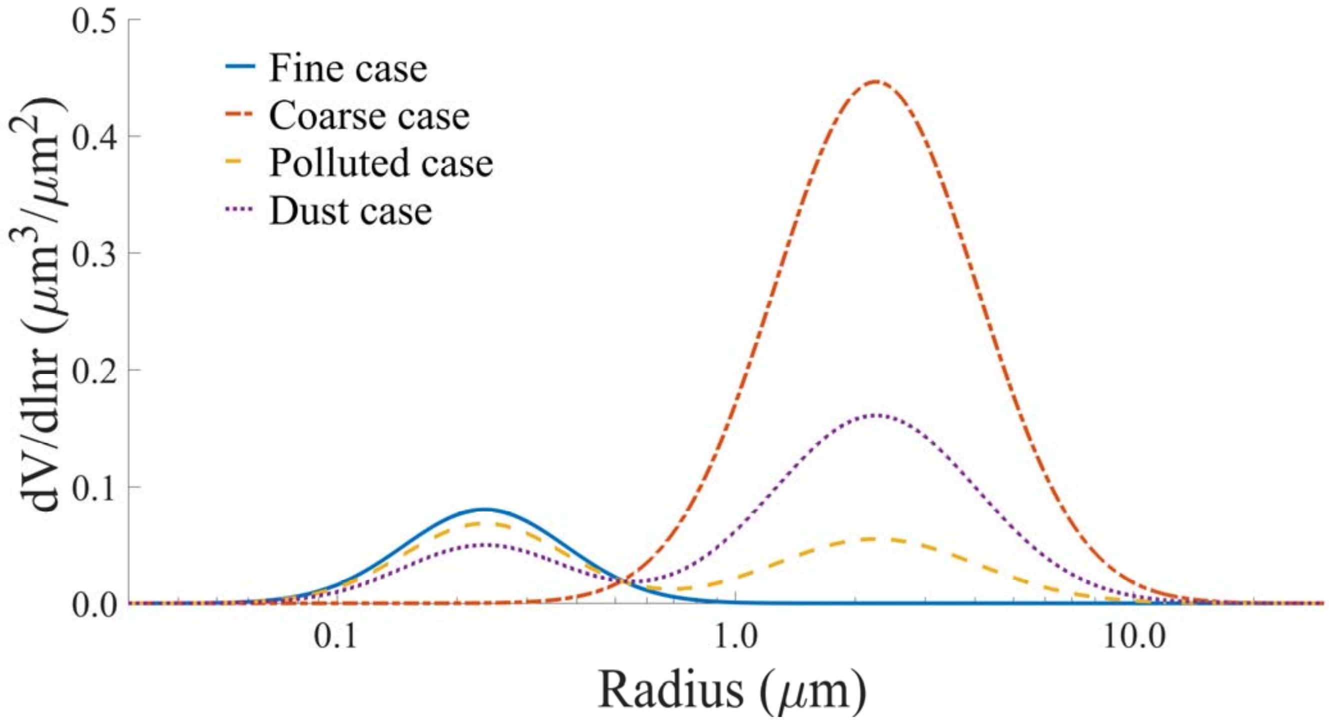

$$\frac{dV}{d\ln r} = \frac{V_0^{\mathrm{f}}}{\sqrt{2\pi}\ln\sigma_g^{\mathrm{f}}}\exp\left[-\frac{\left(\ln r - \ln r_V^{\mathrm{f}}\right)}{2\ln^2\sigma_g^{\mathrm{f}}}\right] + \frac{V_0^{\mathrm{c}}}{\sqrt{2\pi}\ln\sigma_g^{\mathrm{c}}}\exp\left[-\frac{\left(\ln r - \ln r_V^{\mathrm{c}}\right)}{2\ln^2\sigma_g^{\mathrm{c}}}\right]$$

✓ Based on climatology analyses of **Sun-sky radiometer observation network (SONET)** measurements, for the polluted and dust aerosols, we assume that these 2 aerosol cases are mixed with different relative percentage between the fine and coarse modes (**Li et al., BAMS, 2018**).

➢ Surface BRDF for simulations

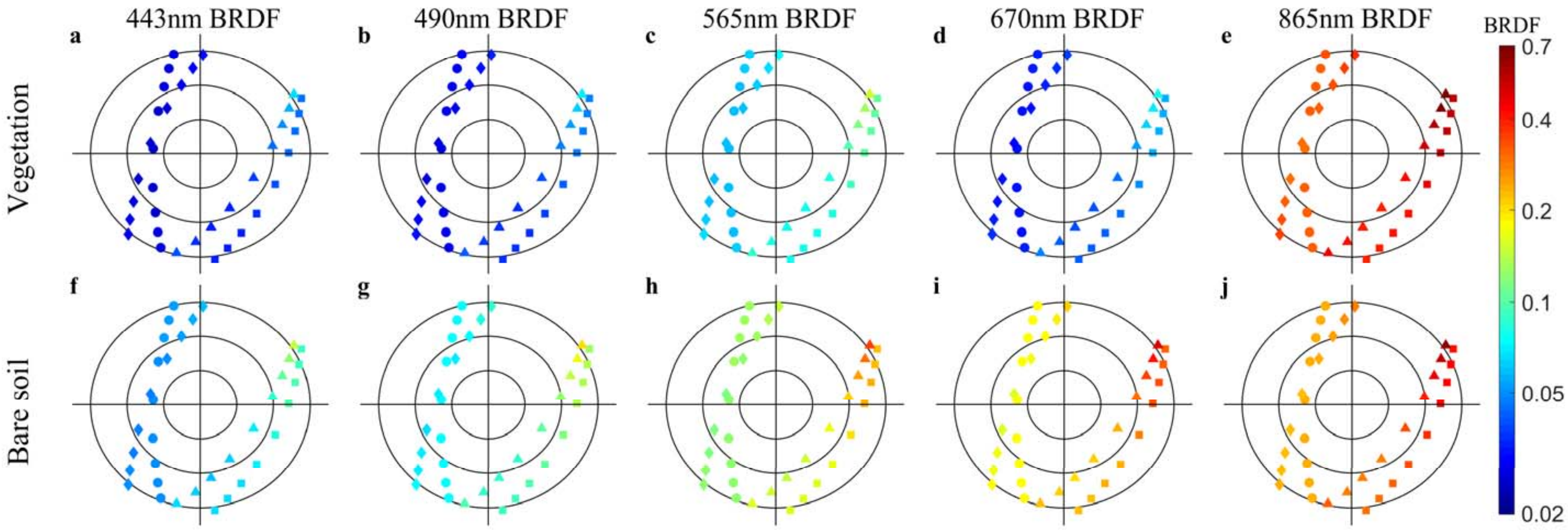

Kernel-driven Ross-Li BRDF model:

$$r_\lambda(\mu_0, \mu_v, \phi) = f_{\text{iso}}(\lambda) + k_1(\lambda) f_{\text{geom}}(\mu_0, \mu_v, \phi) + k_2(\lambda) f_{\text{vol}}(\mu_0, \mu_v, \phi)$$

Improved BRDF model:

$$r_\lambda(\mu_0, \mu_v, \phi) = f(\lambda)[1 + k_1 f_{\text{geom}}(\mu_0, \mu_v, \phi) + k_2 f_{\text{vol}}(\mu_0, \mu_v, \phi)]$$

➢Surface BPDF for simulations

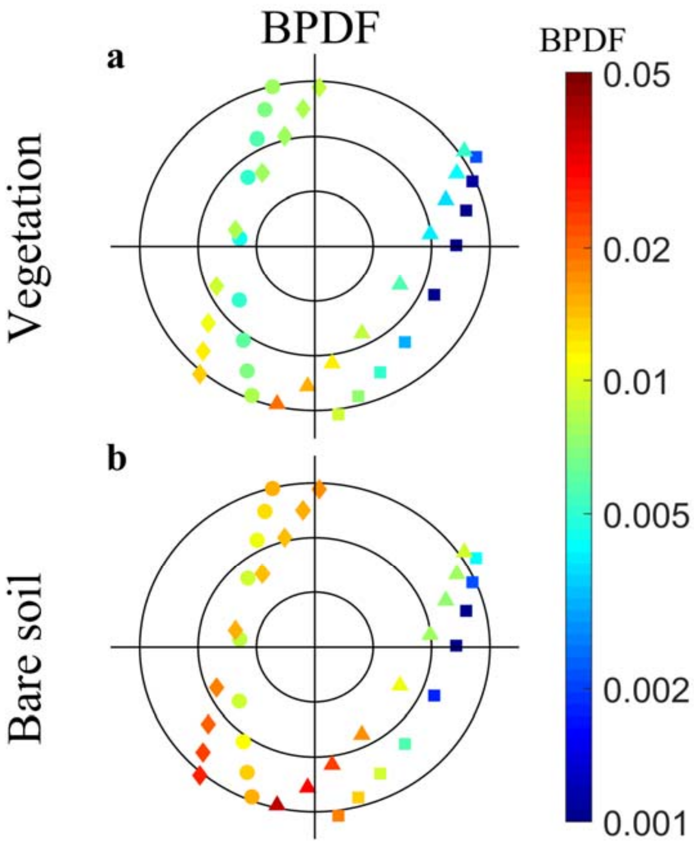

$$R_p^s(\mu_0, \mu_\mathrm{v}, \varphi) = \rho_{\mathrm{Maignan}}\, \mathbf{F}_{1,2}(\gamma, n_i)$$

$$\rho_{\mathrm{Maignan}} = \frac{C \exp(\tan\gamma)\exp(\mathrm{NDVI})}{4(\mu_0 + \mu_\mathrm{v})}$$

- ✓ The surface-polarized reflectance is regarded as independent on the wavelength.

➢ Simulated TOA reflectance of DPC

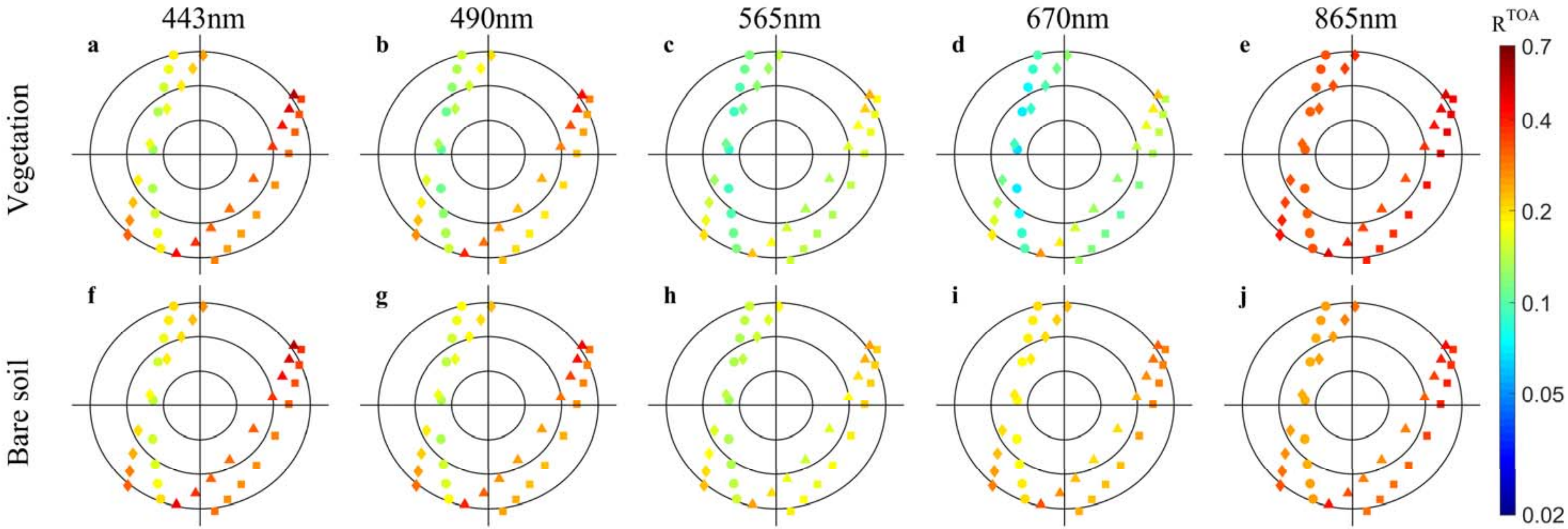

The simulations are for polluted case with AOD = 0.6 at 550nm.

Li, Z., et al. (2018), **Directional Polarimetric Camera (DPC): Monitoring aerosol spectral optical properties over land from satellite observation,** ***JQSRT*****,** ***218*****, 21-37**

➢ Simulated TOA polarized reflectance of DPC

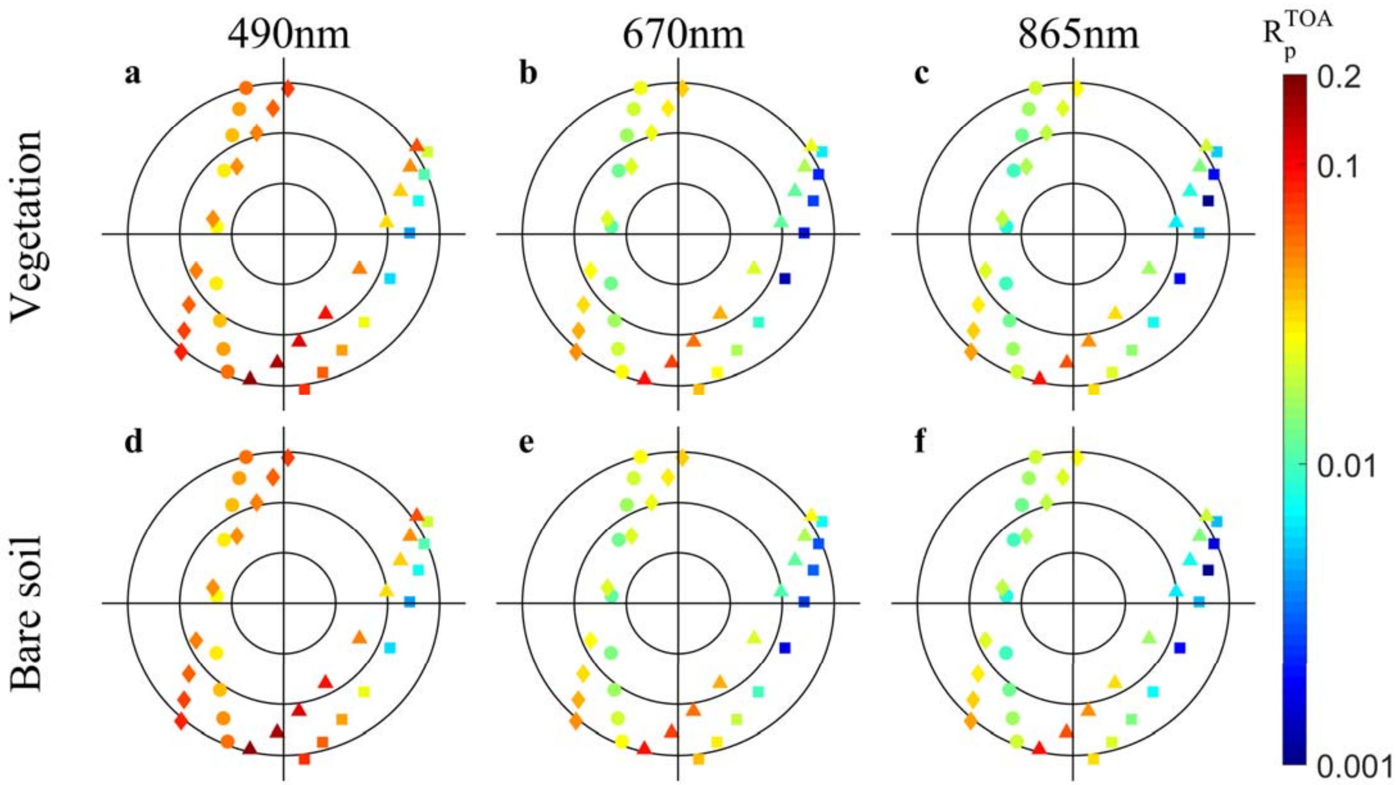

The simulations are for polluted case with AOD = 0.6 at 550nm.

Li, Z., et al. (2018), Directional Polarimetric Camera (DPC): Monitoring aerosol spectral optical properties over land from satellite observation, *JQSRT*, *218*, 21-37

➢ Information content analysis

❖ To test the retrieval capability from DPC, we introduce the averaging kernel matrix:

$$\mathbf{A} = (\mathbf{K}^T \mathbf{S}_\epsilon^{-1} \mathbf{K} + \mathbf{S}_\mathrm{a}^{-1})^{-1} \, \mathbf{K}^T \mathbf{S}_\epsilon^{-1} \mathbf{K}$$

- ✓ The trace of $\mathbf{A}$ is equivalent to the number of independent pieces of information from the TOA measurements, also called the degree of freedom for signal (**DFS**).
- ✓ As long as the DFS result $\mathbf{A}_{i,i} > 0.5$, we assume that the retrieval of parameter x_i could be carried out.

➢ Performance of improved BRDF model

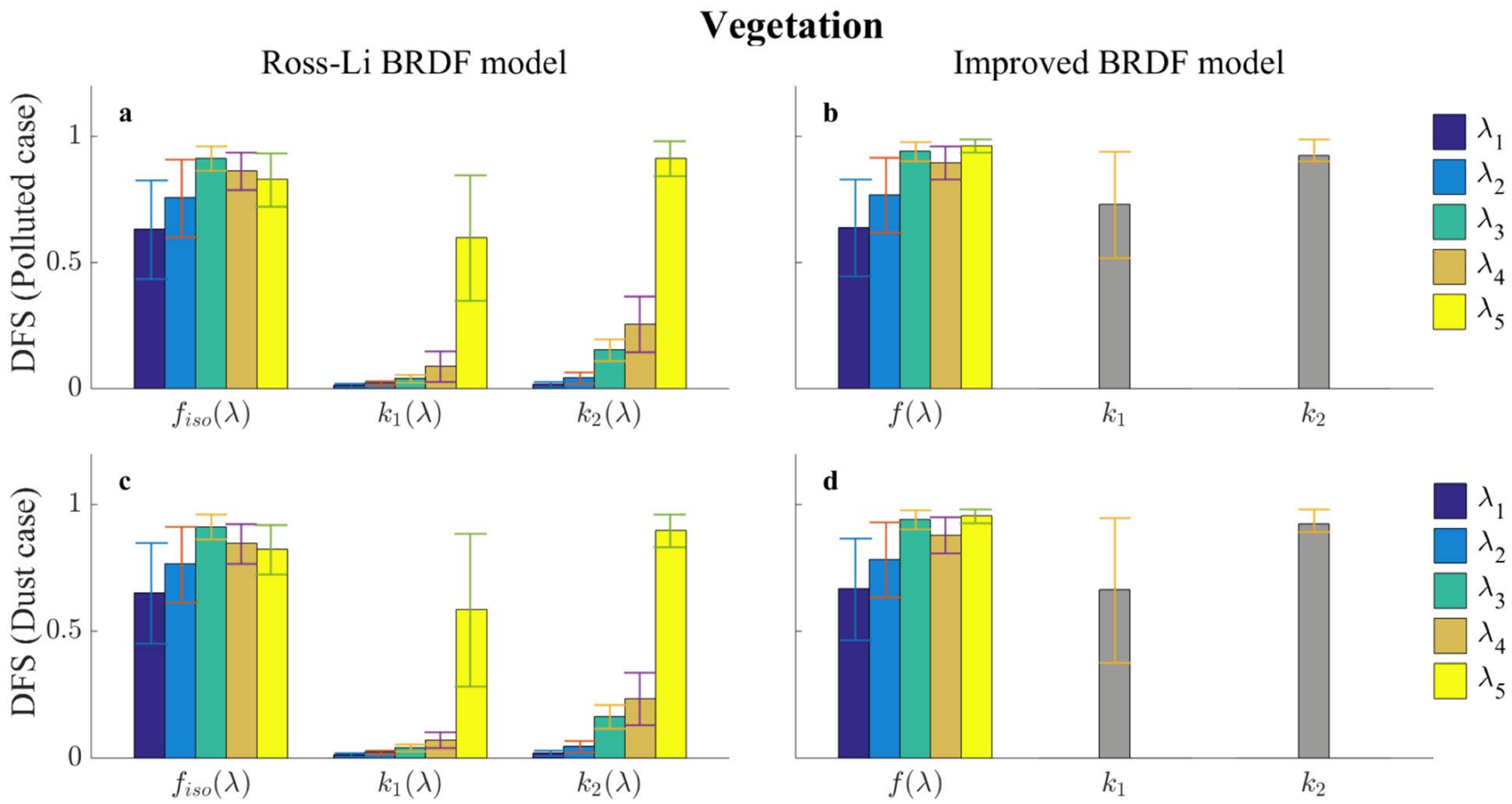

$$r_\lambda(\mu_0,\mu_v,\phi) = f_{\mathrm{iso}}(\lambda) + k_1(\lambda) f_{\mathrm{geom}}(\mu_0,\mu_v,\phi) + k_2(\lambda) f_{\mathrm{vol}}(\mu_0,\mu_v,\phi)$$

$$r_\lambda(\mu_0,\mu_v,\phi) = f(\lambda)[1 + k_1 f_{\mathrm{geom}}(\mu_0,\mu_v,\phi) + k_2 f_{\mathrm{vol}}(\mu_0,\mu_v,\phi)]$$

➢ Performance of improved BRDF model

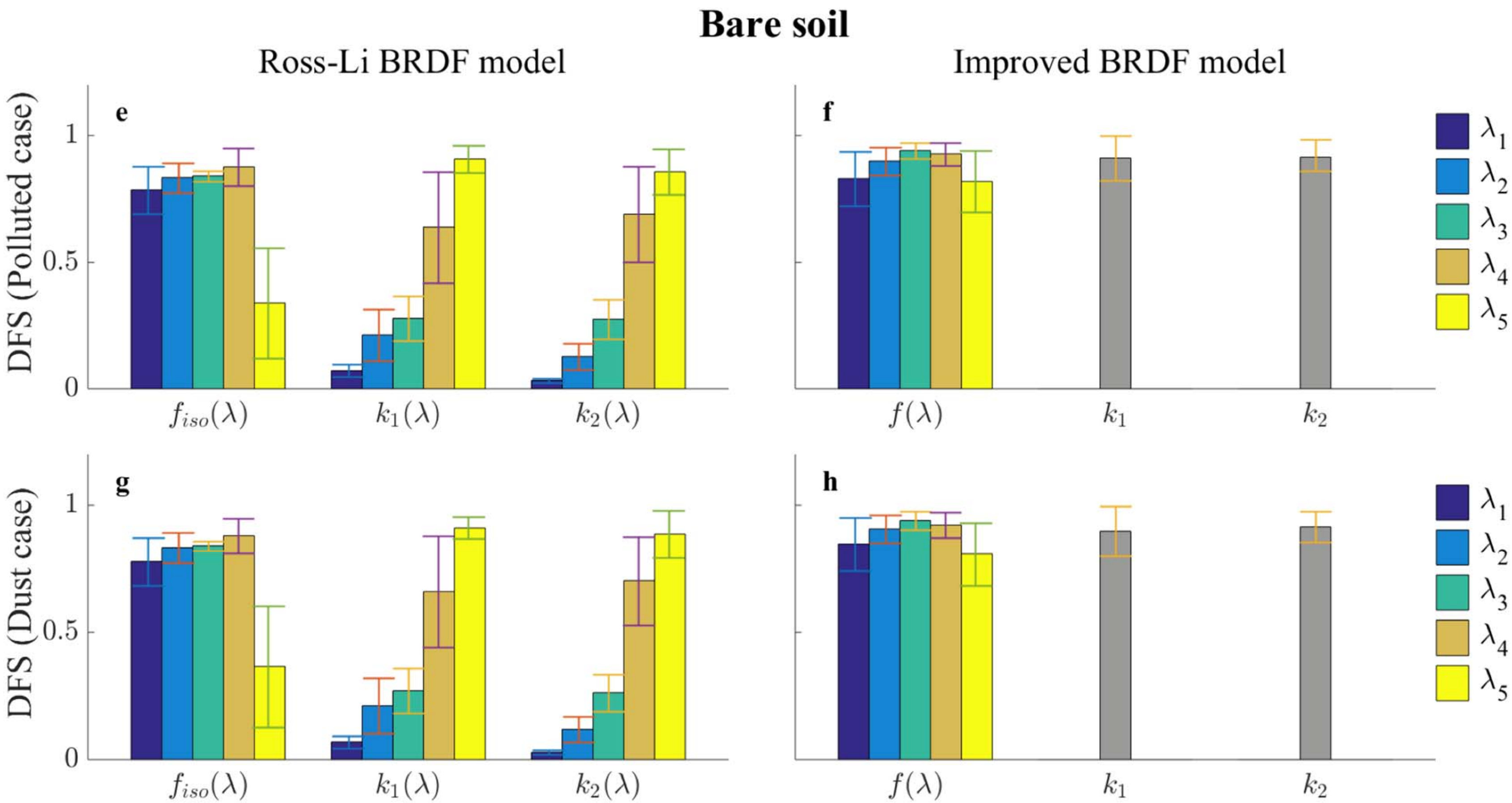

$$r_\lambda(\mu_0,\mu_v,\phi) = f_{\text{iso}}(\lambda) + k_1(\lambda) f_{\text{geom}}(\mu_0,\mu_v,\phi) + k_2(\lambda) f_{\text{vol}}(\mu_0,\mu_v,\phi)$$

$$r_\lambda(\mu_0,\mu_v,\phi) = f(\lambda)[1 + k_1 f_{\text{geom}}(\mu_0,\mu_v,\phi) + k_2 f_{\text{vol}}(\mu_0,\mu_v,\phi)]$$

➢Retrieval capability for typical cases

- ✓ For the 2 realistic aerosol types (polluted and dust), the retrieval performances are all quite good in most cases.

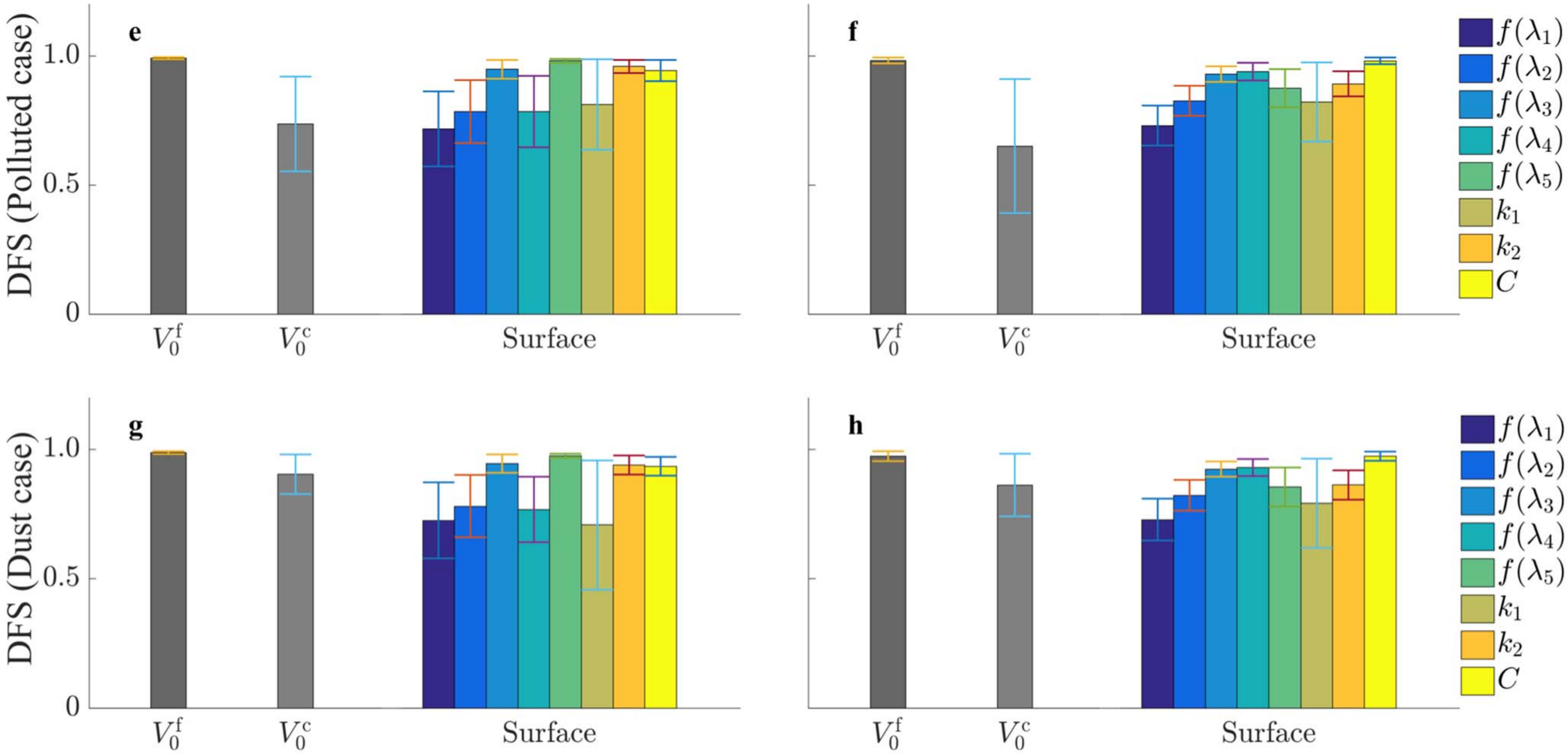

$$r_\lambda(\mu_0, \mu_v, \phi) = f(\lambda)[1 + k_1 f_{\mathrm{geom}}(\mu_0, \mu_v, \phi) + k_2 f_{\mathrm{vol}}(\mu_0, \mu_v, \phi)]$$

➢ Retrieval capability for aerosol spectral optical properties

Equivalent DFS of $\tau_a(\lambda)$	Vegetation	Bare Soil
Fine case	0.99	0.98
Coarse case	0.91	0.88
Polluted case	0.87	0.84
Dust case	0.91	0.89

- ✓ Over various surface types, the spectral aerosol parameters $\tau_a(\lambda)$ can be well determined (Li et al., JQSRT, 2018).
- ✓ The pure fine particles cases can be perfectly determined, while DFS of the pure coarse particle cases are relatively lower.

Outline

- 1. Polarimetric satellite remote sensing
- 2. Inversion framework for DPC/GF-5
- **3. Aerosol retrieval & preliminary validation**

➢ First global map of DPC/GF-5

❖ **Intensity data at 490, 565, 670 nm**

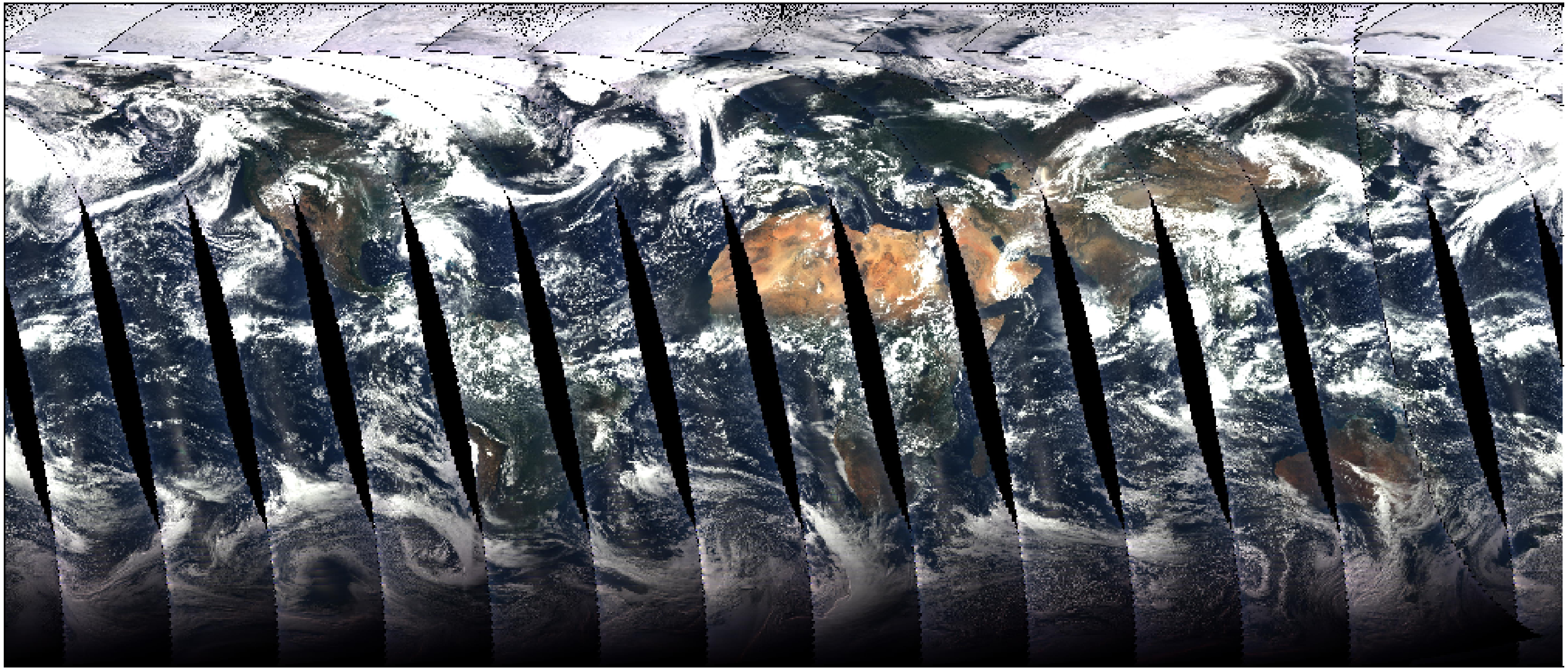

❖ Polarimetric data at 490, 670, 865 nm

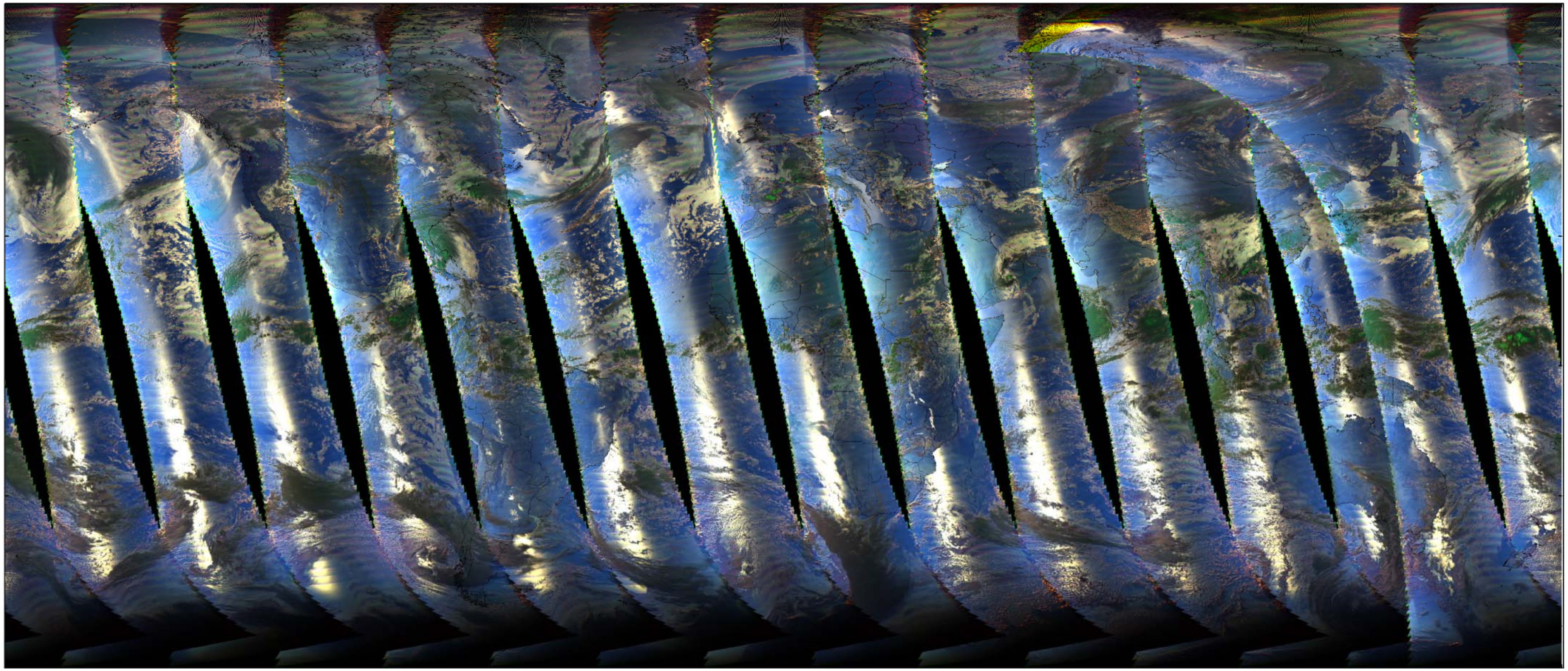

First global map of fine-mode AOD (AODf) retrieved from DPC/GF-5

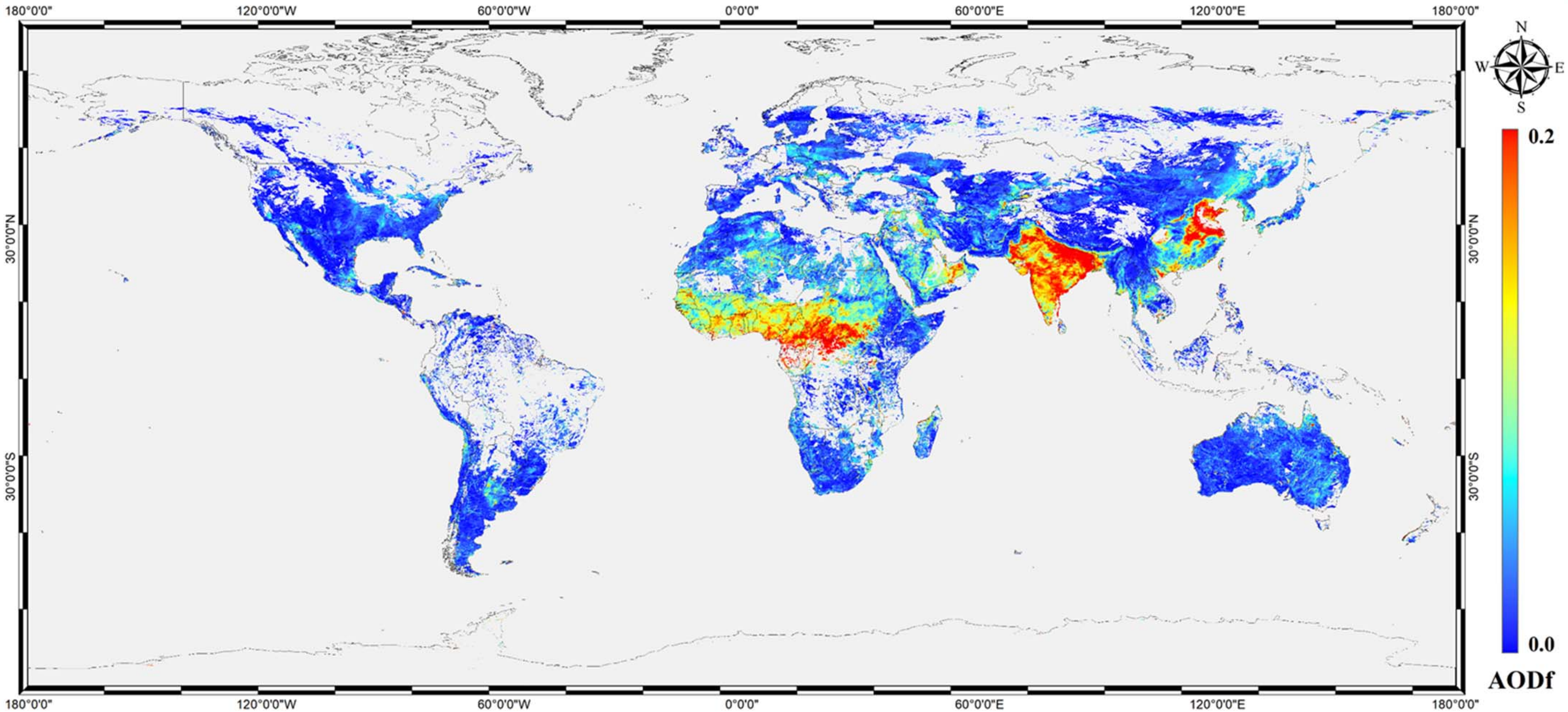

高分五号多角度偏振成像仪（DPC）

0 2,500 5,000 7,500 10,000 Kilometers

制图单位：中国科学院空天信息研究院

数据时间：2018年11月23日—11月30日

制图时间：2019年4月9日

❖ Comparison of AODf from DPC and POLDER in Beijing

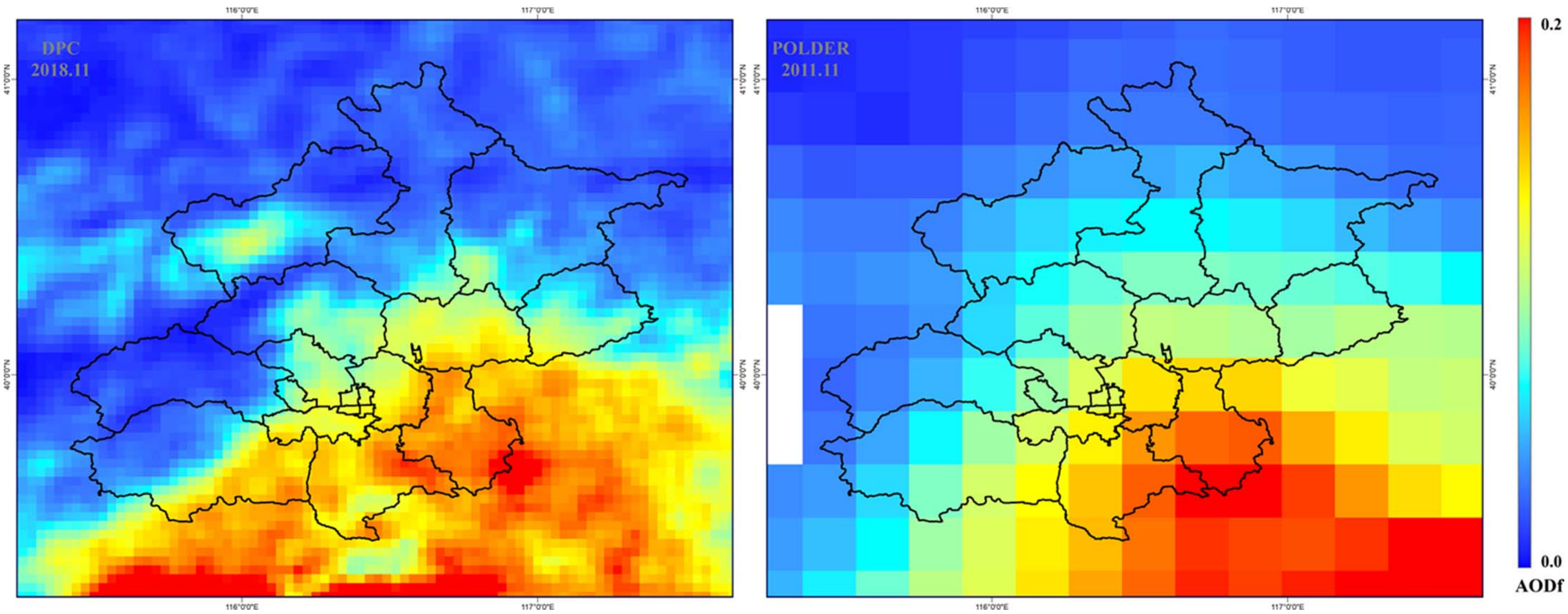

3.3km of DPC in Nov. 2018

18.5km of POLDER in Nov. 2011

❖ **Comparison of AODf from DPC and POLDER in China, India and Africa**

3.3km of DPC in Nov. 2018

18.5km of POLDER in Nov. 2011

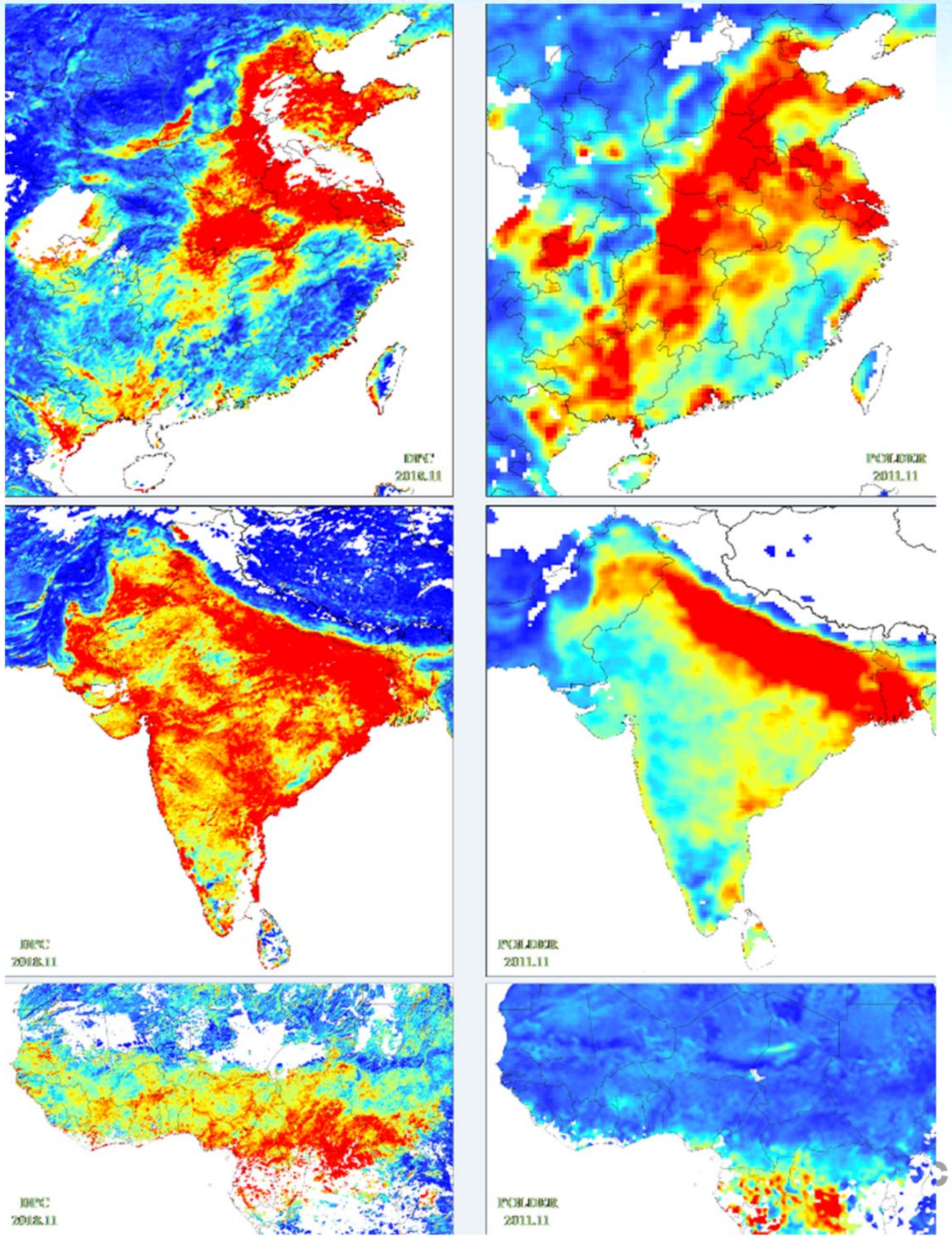

➤ The polarized Sun-sky radiometer network (SONET)

Observation of polarized sky radiance from 340 to 1640 nm every 1 hour together with aerosol, cloud & water vapor contents at 17 sites.

http://sonet.ac.cn

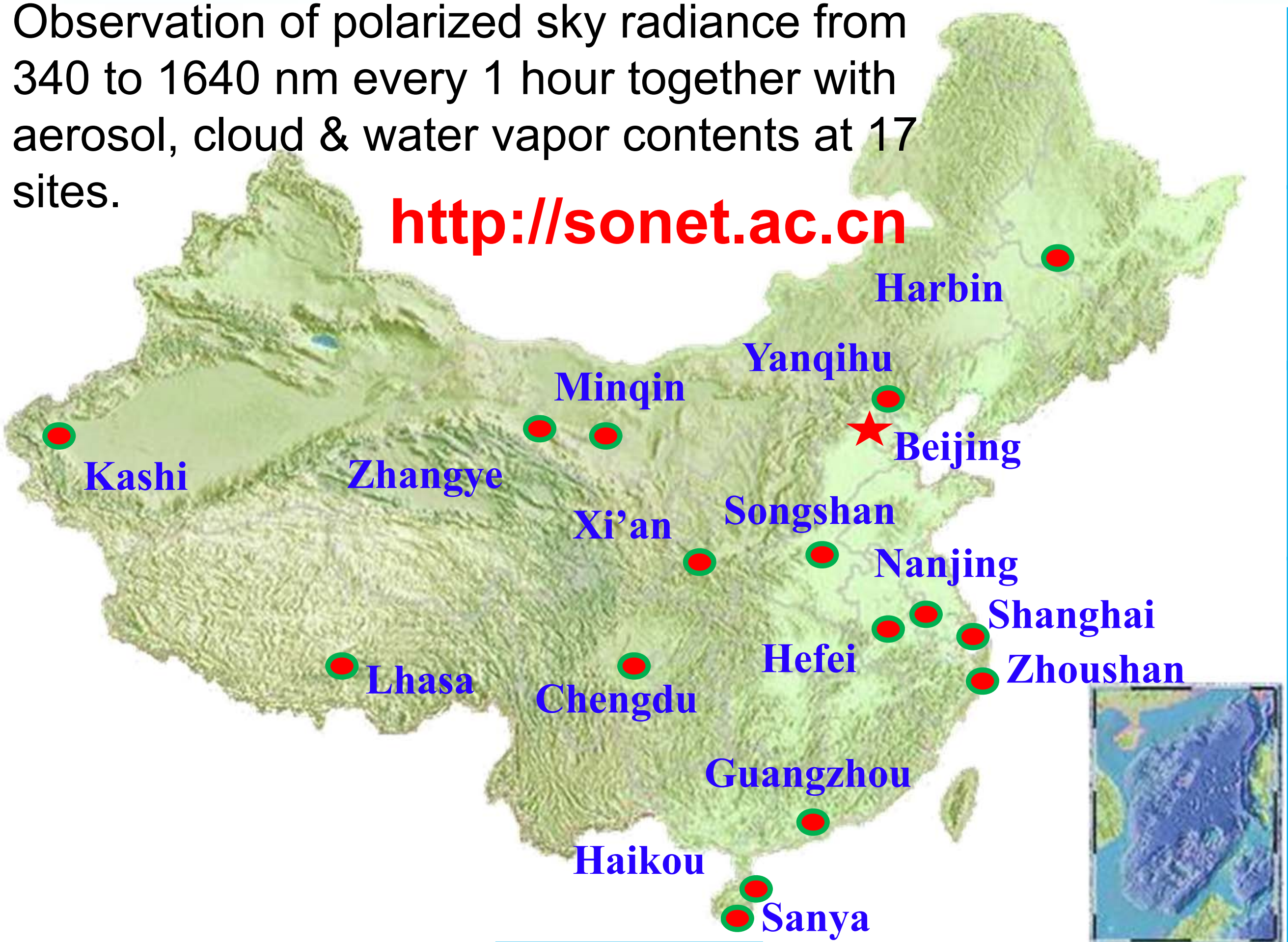

❖ SONET instrument parameters and sites

TABLE 1. Wavelengths, bandwidths, and polarization of the sun–sky radiometer CE318-DP. FWHM = full width at half maximum.

Bands (nm)	340	380	440	500	675	870	936	1,020	1,640
FWHM (nm)	2	4	10	10	10	10	10	10	25
Polarization (yes/no)	Yes	Yes	Yes	Yes	Yes	Yes	No	Yes	Yes

Climate	Site	Location	Alt (m)	Start time	Aerosol characteristics
Tropical	Sanya	18.3°N, 109.4°E	29	Aug 2014	Maritime + urban
	Haikou	20.0°N, 110.3°E	22	Mar 2014	Maritime + urban
Temperate	Guangzhou	23.1°N, 113.4°E	28	Nov 2011	Maritime + urban/PRD region
	Zhoushan	29.9°N, 122.1°E	29	Jan 2012	Maritime + urban
	Shanghai	31.3°N, 121.5°E	84	Mar 2013	Maritime + urban/YRD region
	Hefei	31.9°N, 117.2°E	36	Jan 2013	Urban/YRD region
	Nanjing	32.1°N, 119.0°E	52	Jan 2013	Urban/YRD region
	Chengdu	40.6°N, 104.0°E	510	May 2013	Urban (basin)
	Songshan	34.5°N, 113.1°E	475	Nov 2013	Urban + dust
	Xi'an	34.2°N, 108.9°E	389	May 2012	Urban + dust
Continental	Beijing	40.0°N, 116.3°E	59	Mar 2010	Urban/Beijing–Tianjin–Hebei region
	Harbin	45.7°N, 126.6°E	223	Dec 2013	Urban
Dry	Minqin	38.8°N, 100.3°E	1,589	Feb 2012	Dust
	Zhangye	38.6°N, 103.0°E	1,364	Jul 2012	Dust
	Kashi	39.5°N, 75.9°E	1,320	Jun 2013	Dust
	Lhasa	29.6°N, 91.2°E	3,678	Sep 2013	Background

❖ SONET data products

Products	Description	Unit
AOD (λ)	Aerosol optical depth (340, 380, 440, 500, 675, 870, 1,020, and 1,640 nm)	—
AE	Ångström exponent (440–870 nm)	—
FMF	Fine-mode fraction of aerosol optical depth (500 nm)	—
SSA (λ)	Single-scattering albedo (440, 675, 870, and 1,020 nm)	—
F_{11} (λ)	Scattering phase function (440, 675, 870, and 1,020 nm)	—
$-F_{12}$ (λ)	Polarization phase function (440, 675, 870, and 1,020 nm)	—
g (λ)	Asymmetry factor (440, 675, 870, and 1,020 nm)	—
S (λ)	Lidar ratio (440, 675, 870, and 1,020 nm)	—
$dV/d\ln r$	VPSD with 22 bins for radius from 0.05 to 15.0 μm	$\mu m^3\ \mu m^{-2}$
n (λ)	Refractive index (real part) (440, 675, 870, and 1,020 nm)	—
k (λ)	Refractive index (imaginary part) (440, 675, 870, and 1,020 nm)	—
r_{eff}	Effective radius (total, fine, and coarse modes)	μm
V	Volume concentration (total, fine, and coarse modes)	$\mu m^3\ \mu m^{-2}$
NS (%)	Percentage of nonspherical particles	—
RF	Shortwave aerosol radiative forcing (0.3–2.8 μm) at TOA or BOA	$W\ m^{-2}$
RFE	Shortwave aerosol radiative forcing efficiency [i.e., RF normalized by AOD (550 nm)]	$W\ m^{-2}$
AW (%)	Percentage of mass concentration of water uptake of aerosols	—
FS (%)	Percentage of mass concentration of fine-mode scattering components (e.g., sulfate, nitrate and light non-absorbing organic matters)	—
CM (%)	Percentage of mass concentration of coarse-mode components (dust or sea salt)	—
BrC (%)	Percentage of mass concentration of brown carbon components	—
BC (%)	Percentage of mass concentration of black carbon components	—

Li, Z., et al. (2018), Comprehensive study of optical, physical, chemical and radiative properties of total columnar atmospheric aerosols over China: An overview of Sun-sky radiometer Observation NETwork (SONET) measurements, *BAMS*, 99(4), 739-755

❖ SONET volume particle size distribution

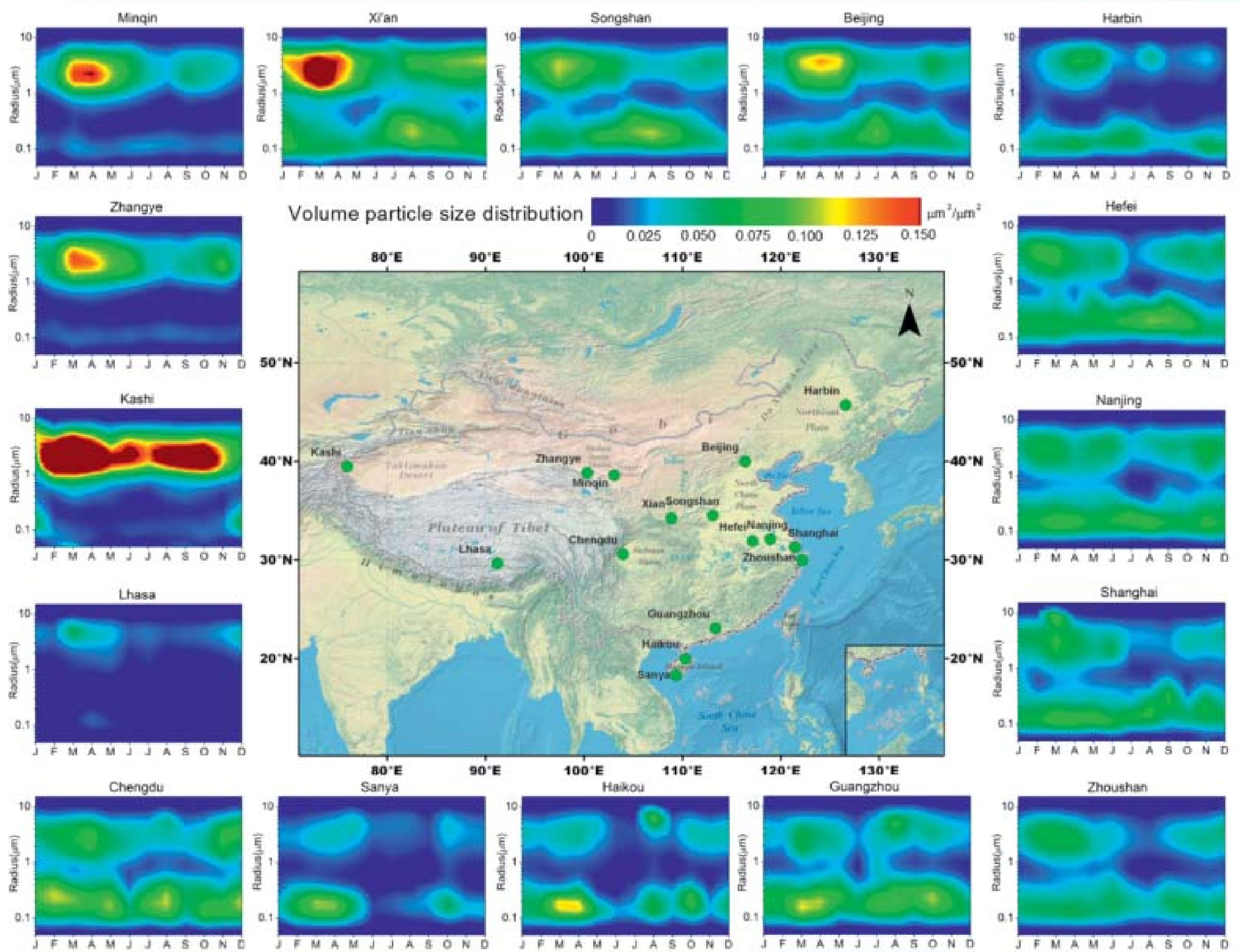

Li, Z., et al. (2018), Comprehensive study of optical, physical, chemical and radiative properties of total columnar atmospheric aerosols over China: An overview of Sun-sky radiometer Observation NETwork (SONET) measurements, *BAMS*, 99(4), 739–755

➢ Validation of AODf from DPC/GF-5

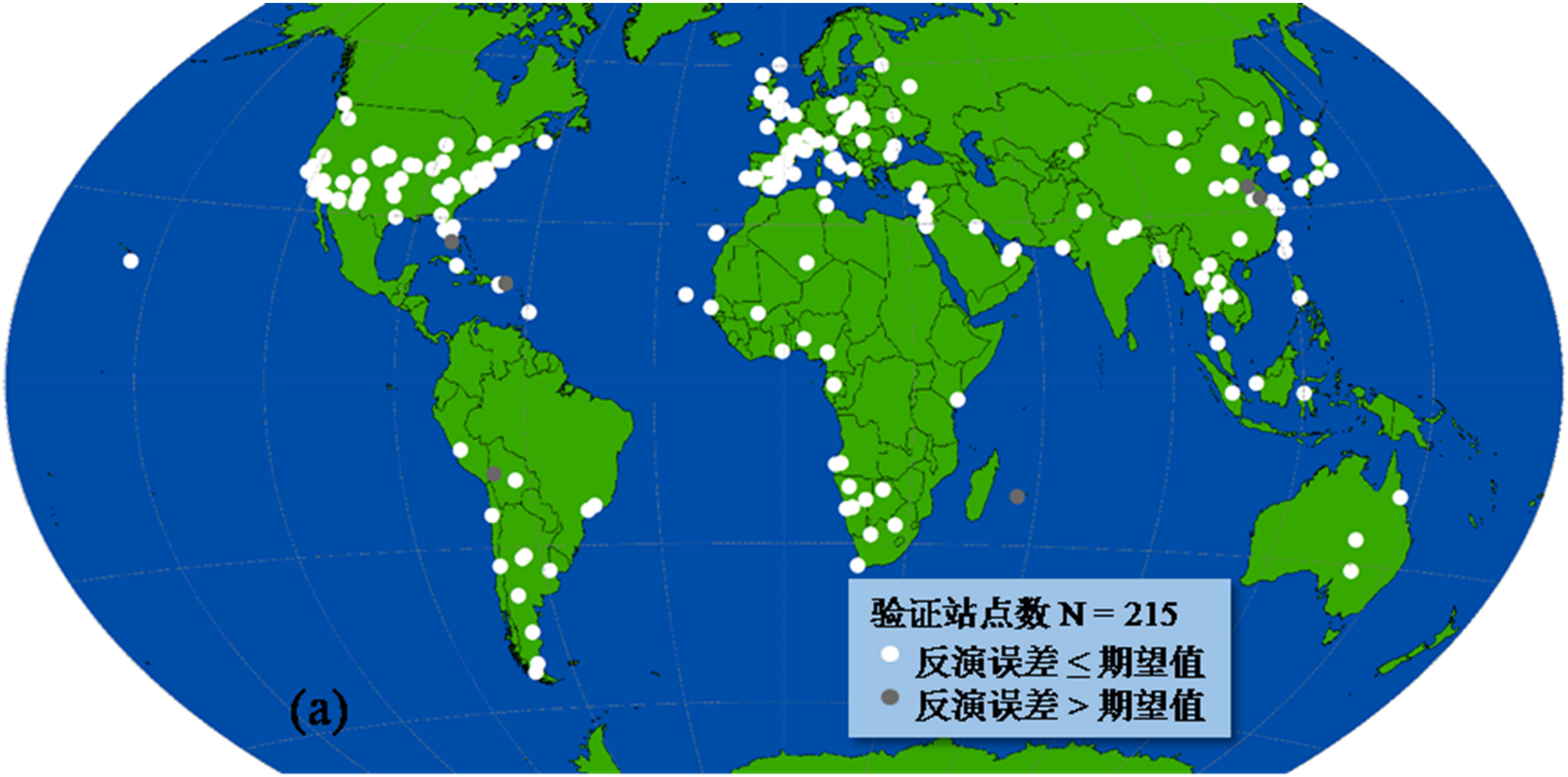

N = 215
y = 0.772*x+0.05
R = 0.908, RSE = 0.028, MAE = 0.009

Thank you！

Aerospace Information Research Institute(AIR)
Chinese Academy of Sciences(CAS)

www.aircas.ac.cn